Blended Wing' CFD Analysis: Aerodynamic Coefficients.

G. Salazar-Jiménez, H. A. López-Aguilar, J. A. Gómez, A. Chazaro-Zaharias, A. Duarte-Moller

and A. Pérez-Hernández

***Abstract*—:** This document is focused in the analysis of the aerodynamic behavior of the airfoil and wing geometry used in an unmanned aerial vehicle (UAV) named "Cenzontle", whose operating conditions rank between 300,000 and 400,000 Re. The wing geometry is compound of three sections, a rectangular one in the middle of the wingspan and two changes of trapezoidal geometries at the tips. The wing utilizes the airfoil called Pinefoil, a novel geometry obtained by interpolation of the S1223 and CH10 airfoils. Through Computational Fluid Dynamics (CFD) simulations, the lift and drag coefficients are estimated as well as the aerodynamic forces on straight and leveled flight in order to calculate the payload of the aircraft. Additionally, the object of study is rotated on its 3 axis, representing the roll, pitch and yaw movements. By applying a statistical analysis of response surface, it is possible to estimate the lift generated while turning the airplane in order to avoid the stall of the wing. The CFD tools represent an accurate option to estimate these parameters with precision.

***Keywords*—**CFD, pitch, stall, UAV

I. Introduction

MOST of the theory of aircraft design is focuses on airfoils at high operational speeds, over 300 km/hr and with Reynolds numbers over 2 x 106 [1, 2]. Some airfoils designed to operate at low Reynolds such as NACA 4412 and Selig 1223 have been studied using the CFD software, calculating coefficients, pressure distribution and speeds around each airfoil. [3-6]. There is free software that focus on studying airfoils at low Reynolds numbers, such as the XFLR5 [5, 7]. Nevertheless, the values obtained through this software are not accurate, especially for airfoils designed and simulated through the interpolation module of XFLR5.

As part of the design for more efficient UAVs, new airfoils are implemented looking for a greater aerodynamic efficiency. For this, it is necessary to generate novel airfoils based on former geometries, in order to take advantage of each of them. Through CFD simulation, fluid dynamic behavior around the subject has been studied, calculating the values of aerodynamic coefficients Cl and Cd on the airfoil and wing geometry [8, 9].

Cenzontle's wing geometry is build up by three sections, the geometry changes on the wing produce a blended surface that differs from the traditional corrections for wing geometries. [1, 10-12]. This work analyzes, through CFD software, the behavior of a mixed wing surface comparing the Cl and Cd coefficients in relation to the incidence angle.

II. Problem Formulation.

In an aircraft there are four main forces: Lift (L), Drag (D), Weight (W) and Thrust (T). Out of which L and D are calculated as follows:

$$L = \frac{1}{2}\rho V^2 S C_l \quad (1)$$

$$D = \frac{1}{2}\rho V^2 S C_d \quad (2)$$

Where:

L= Lift force.
D= Drag force.
ρ =air density.
V^2= velocity
S= wing surface.
C_l= Lift coefficient.
C_d= Drag Coefficient.

These coefficients display different values upon changing their incidence with respect to the fluid, which is analyzed with polar graphics. Wing geometry, besides changing its attack angle it can vary its position with respect to its longitudinal and vertical axis starting its turn.

The lift resultant for steady level turns, is decomposed in a

This work was supported in part by the CONACYT (Consejo Nacional de Ciencia y Tecnologia) and CIMAV (Centro de Investigación en Materiales Avanzados)

G. Salazar-Jiménez is with Universidad Aeronautica en Queretaro, Carretera Estatal 200, Parque Aeroespacial Queretaro, Colon, Queretaro, Mexico. C.P. 76278 (e-mail: gamasalazar27@gmail.com)

H. A. López-Aguilar is with Centro de Investigación en Materiales Avanzados, Miguel de Cervantes 120, Complejo Industrial Chihuahua, Chihuahua, C.P. 31136, México (e-mail: hector.lopez@cimav.edu.mx)

J. A. Gómez is with Universidad Autónoma de ciudad Juárez, Avenida del charro 450. Col. Partido Romero, C.P. 32310, México (e-mail: joralgomez74@gmail.com)

A. Chazaro-Zaharias is with Universidad Aeronautica en Queretaro, Carretera Estatal 200, Parque Aeroespacial de Queretaro, Colon, Queretaro, Mexico. C.P. 76278 (e-mail: adriana.chazaro@gmail.com)

A. Duarte-Moller is with Centro de Investigación en Materiales Avanzados, Miguel de Cervantes 120, Complejo Industrial Chihuahua, Chihuahua, C.P. 31136, México (e-mail: alberto.duarte@cimav.edu.mx)

A. Pérez-Hernández is with Centro de Investigación en Materiales Avanzados, Miguel de Cervantes 120, Complejo Industrial Chihuahua, Chihuahua, C.P. 31136, México (corresponding author phone: 52 614439-1100 e-mail: antonino.perez@cimav.edu.mx)

horizontal component defined by the Ec. 3, and a vertical as shown in the Ec. 4. [13- 15].

$$L\cos\beta = W \quad (3)$$

$$L\,\mathrm{sen}\,\beta = \frac{WV^2}{gR} \quad (4)$$

Where:

L=Lift force.
β= Bank angle
W=total weight of the aircraft.
V= velocity
R= Turning radius

The turning radius can be found by isolating R from Ec. 4, as follows:

$$R = \frac{WV^2}{gL\sin b} \quad (5)$$

This project considered two specific study cases named: airfoil and wing geometry. The study and selection of the airfoil was made through 2D simulations, while the wing geometry was analyzed through 3D.

A. *Case 1 Airfoil Pinefoil.*

The aircraft Cenzontle was designed for SAE Aero Design Brasil 2016 [16] where the objective is to lift a payload with dimension restrictions, for this reason it was sought that with the used airfoil in the wing geometry, the greater lift and the least drag possible were obtained. The designed aircraft has an empty weight of 2.135 kg, with a wingspan of 1.44m and a height of 0.4 m. The wing surface is 0.75m2 and a mean aerodynamic chord (MAC) of 0.38m.

A Pinefoil airfoil was developed by using the interpolation of the aerodynamic aerofoils S1223 and CH10, airfoils designed to operate under low Reynolds numbers. Operating conditions were estimated between 300,000 and 400,000 Reynolds for the study case, for this reason it was necessary to study the airfoil and the wing geometry in a specific way to obtain an approximation of the coefficients that consider the viscous effects. [17]. For that, the airfoil was studied in a CFD analysis in 2D as the first case.

B. *Definition of control surface.*

In the analysis of the airfoil (Fig. 1) in 2D, a type "C" domain was used, that is to say, a geometry with a semicircular entrance of 7 m in radius and a rectangular section of 14x10 m. The airfoil subject to study is placed in the center of the semicircle so that the effect of the bondary layer of the walls does not affect the behavior of the fluid in the area near to the profile.

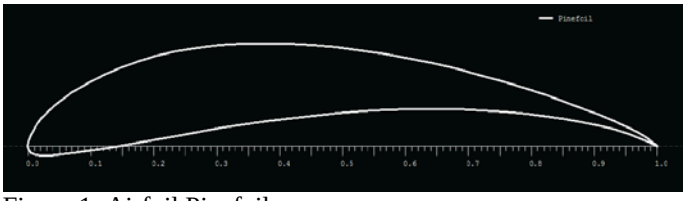

Figure 1: Airfoil Pinefoil.

C. *Mesh analysis.*

In the process of the discretization of the domain it was a priority to refine the area near the airfoil surface, since it is the area where the phenomenon of the shedding of the boundary layer is showing. A comparative analysis between a structured and a non-structured mesh was contemplated. For the structured meshing it was used the "sizing" and "Bias factor" tool on the borders of the domain and airfoil, to generate a meshing type C, which has been found appropriate to simulate fluids around the airfoil. [17, 18]. For the non-structured mesh it was used the "sizing" tool, by adjusting the minimum size of the element over the outline of the studied object.

Using structured meshes a sensitivity analysis was conducted in order to obtain a stable value of the coefficients to an angle of attack of 0°. Using a non-structured meshing the mesh size in the edge of the airfoil was refined to obtain coefficients values similar to those obtained with the structured mesh, elements with minimum length of 0.07 mm in the contours of the airfoil were used, obtaining a mesh of 1.36 x 105 elements as shown in Figure 2.

The structured meshing demands more processing time and presents difficulties to the discretization of the domain when it increases the incidence of the airfoil.

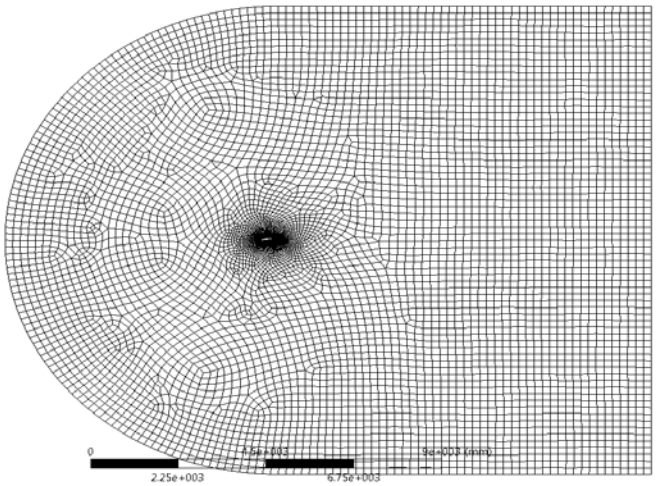

Figure 2: 2D Domain semi-circular with non-structured meshing. The central area is refined with a size of element in the edge of the airfoil of 0.07 mm.

D. *Viscous solution model, boundary conditions, monitors.*

A turbulent phenomenon was considered using the Spalart-Allmaras model, for its solution a pressure based solution model was used. This model is commonly used in CFD simulations of aerodynamic profiles, wings and elements of study within the field of aeronautics; it uses a transport equation for Eddys viscous effects [19].

Inside the domain, the following boundary conditions are defined: "Vel-Inlet"in the region of semicircular entry, "Outflow" to the output of the domain and "Wall" in the contour of the airfoil and upper and lower edge of the domain. Additionally, monitors of Cl and Cd were used during the simulation, these allowed to identify the stability of the solution.

E. Convergence criteria for Case 1:

In the case of study the following convergence criteria were defined:

- The residuals of the equations of continuity and speed of the fluid reached values of $1x10^{-6}$.
- The monitored variables of interest showed stable values regardless of the number of iterations.
- It was confirmed a difference of almost zero between the mass flow of input and output the mass flow.

For the density and viscosity of air the standard values were taken, the speed of the fluid (IAS) was defined between 12 m/s and 16 m/s. The airfoil was analyzed by modifying the angle of attack from 0° to 15° in increments of 3° [5].

F. Design of Experiments (DoE) and response surface (RS).

For the statistical analysis of correspondence between the angle of incidence with the speed of the fluid (IAS), a design of experiments was performed. The variation of the angle of incidence was carried out by means of the rotation of the airfoil ( ) through the operation "rotate", and with the speed IAS were obtained coefficients (Cl and Cd). A DoE type "Central Composite Design" (CCD) was used to generate the design points (DP) and to develop the response surface graphs [20]. The polar graphs of the airfoil (Cl vs and Cd vs) were built up based on this methodology.

G. 2.2 Case 2: Wing geometry.

For this analysis, it was built the wing geometry starting from the aerodynamic profile obtained in the 2D simulation.

For the simulation it was generated a cylinder with one of its sides with a semi spherical shape, placing the wing geometry in the center of the domain.

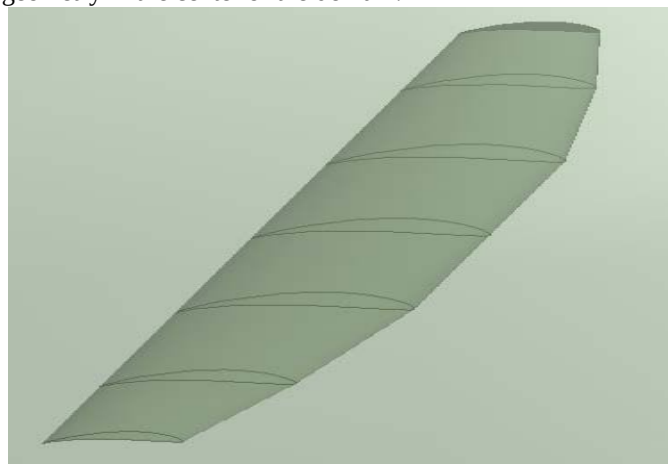

Figure 3: 3D Domain: To analyze wing geometry of Cenzontle.

The 3D Domain (Fig. 3) was discretized using an unstructured tetrahedral mesh. A refinement was considered using the suface sizing" and "body of influence" tools. Since it is a three-dimensional domain, the CFD simulation was performed with a mesh of 8.1×10^6 elements, which is shown in Figure 4. For the analysis in 3D, the solution model, boundary conditions and criteria of convergence, as well as density, viscosity and velocity of the air were similar to the case in 2D.

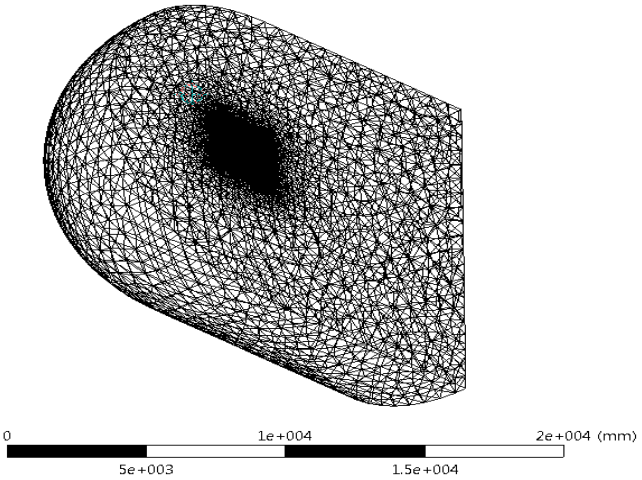

Figure 4: Discretized 3d Domain. The wing geometry is located in the refined central area.

To generate the response surface was used the rotation of the wing with respect to its three axes as input parameters and coefficients (Cl and Cd) as outputs. The rotation about the z-axis represents the angle of attack that varies from 0° to 13° (pitch), while for rotation about the x-axis and y-axis, represent the roll angle and yaw respectively, both of which have a maximum of 30° of rotation. With these input parameters were generated 15 design points that cover the ends of each parameter and the intermediate points according to the DoE type CCD.

The response surface generated is based on a second order polynomial regression. Based on these values it is possible to obtain the variation of the coefficients by rotating the wing in different positions according to the angle of attack. These response surfaces were built to know velocity correction and to maintain the aircraft under design, in straight and leveled flight during turnings.

III. Problem Solution.

A. Case 1: Airfoil Pinefoil

The analysis of the aerodynamic profile allowed the calculation of the tensor fields of the main parameters that describe the phenomenon. The differential of velocities of the bottom surface of the airfoil with respect to the top surface generates differences in pressure creating the lift force on the airfoil. The results focused on analyzing of the critical positions of the airfoil, that is to say, from 0° to 3° degrees of incidence that represent conditions of straight and level flight, and conditions close to the stall of the airfoil, between 12° to 15°. The Contours of pressure and velocities are shown in Figures 5-12.

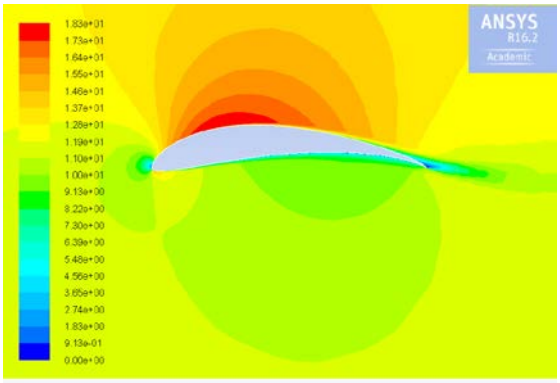

Figure 5: Velocity contours at α=0°

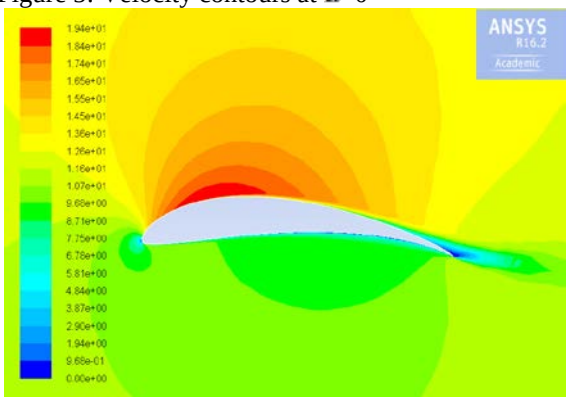

Figure 6: Velocity contours with α=3°

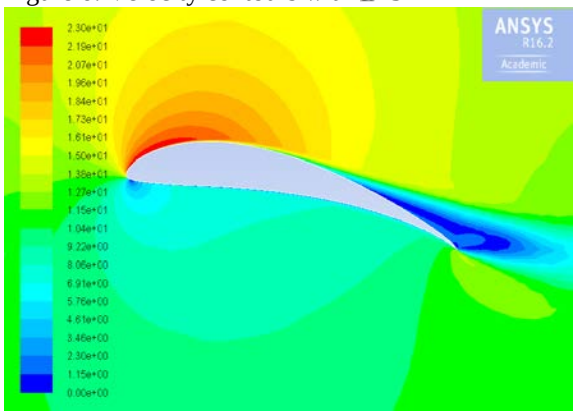

Figure 7: Velocity contours at α=12°

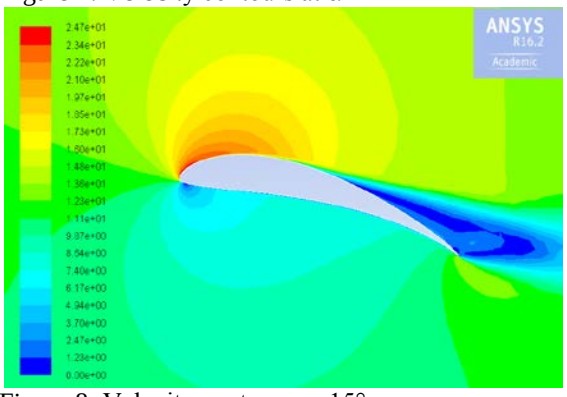

Figure 8: Velocity contours α=15°

The air speed on the upper surface of the airfoil presents an increase as it scrolls toward the trailing edge. When the incidence of airfoil is 0° to 3°, the air reaches its maximum velocity between 15% and 50% of the chord on the upper side (Figures 5 and 6), so that in that area will be generated the greatest differential of pressures of the airfoil. When positioning the airfoil at 3° of incidence, the airflow reaches a speed of 19.4 m/s over the upper surface and above the boundary layer, this value is increases 23 m/s with an incidence of 12° and up to 24.7 m/s by positioning the airfoil at 15° as shown in figures 7 and 8 respectively.

Since it is a cambered airfoil, turbulent phenomena are presented in each of the positions to a lesser or greater magnitude in the region of the trailing edge. From the 6° of incidence, the detachment of the boundary layer starts to be noticeable along the top side, reaching almost the central region of the airfoil to the 15° (Figure 8). This condition increases the drag generated by the airfoil and reduces the lift generated, in comparison with an incidence angle of 12°, which indicates that the airfoil is in a condition of "stall".

The fluid presents lower velocities along the lower surface, a situation associated with the geometry of the airfoil that causes a deceleration of the fluid in the leading edge when the air enter in contact with the airfoil. The pressures are shown distributed along the chord of the airfoil at smaller angles. The center of pressure between 0° and 3° is located at approximately the 30% of the chord; that is to say, the pressure differential is greater at that location, as shown in Figures 9 and 10.

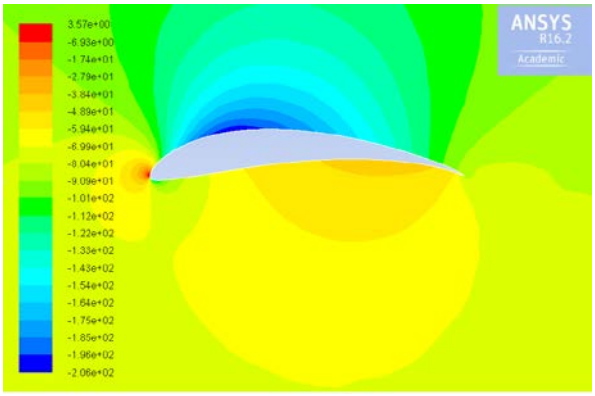

Figure 9: Static pressure contours at α=0°

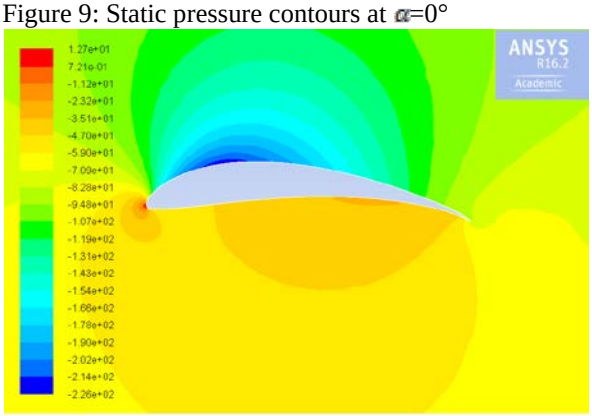

Figure 10: Static pressure contours at α=3°

Upon increasing the incidence of the airfoil, the center of pressure is concentrated toward the leading edge (Figure 11 and 12).A region of stagnation is produced on the leading edge caused by the fluid contact with the airfoil, as it increases the incidence, this point moves towards the lower surface. moved

to the lower surface.

Table 2: Pinefoil coefficients (Cl and Cd)at two speeds.

α	Cl		Cd	
	12 m/s	**16 m/s**	**12 m/s**	**16 m/s**
0	1.1075	1.1162	0.0206	0.0199
3	1.3872	1.4006	0.0256	0.0246
6	1.6395	1.6544	0.0326	0.0313
9	1.8185	1.8384	0.0442	0.0424
12	1.9090	1.9276	0.0661	0.0637
15	1.8912	1.9117	0.1048	0.1017

Table 2 contains the values of Cl and Cd obtained for Pinefoil for two different airspeeds. Based on these results, it is possible to define an angle of attack of 3° as the ideal for straight and level flight producing a Cl 1.38 to 12 m/s. In this position, the airfoil reaches its maximum aerodynamic efficiency with a value of 54.18, which is obtained by dividing the Cl on CD and it represents the relationship of lifting equipment per unit of drag generated. The stall angle of the airfoil is estimated at 12°, for values of C_{l_m}1.9 and a Cd of 0.06.

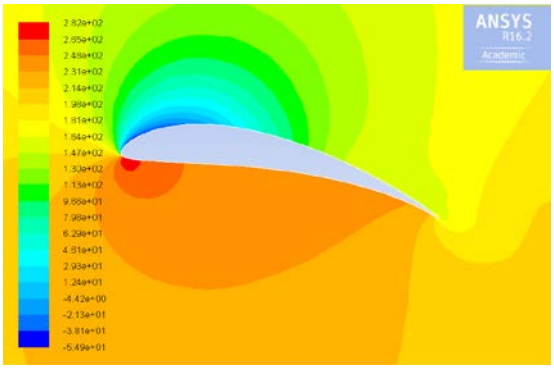

Figure 11: Static pressure contours at α=12°

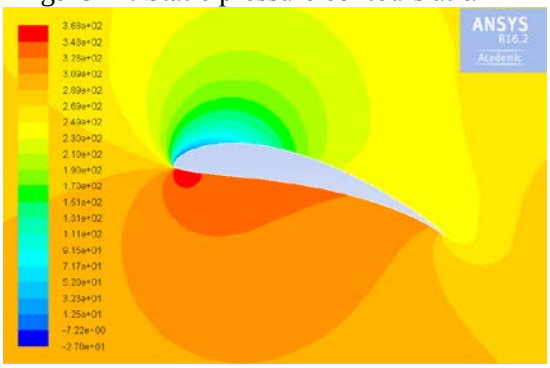

Figure 12: Static pressure contours at α=15°

Polar graphs of the airfoil obtained through the response surface are shown in Figures 13 and 14. The increase in the angle of attack was made taking as the origin the leading edge of the airfoil. The values of Cl remain similar to those estimated by Fluent in a rangeof 0° and 6°, however, to greater angles, the Cl has values below the CFD analysis carried out in Fluent. For its part, the Cd (Figure 14) reaches a value equivalent to 12° since 6° of incidence, so that the drag values are overestimated in comparison to the previous simulation in Fluent.

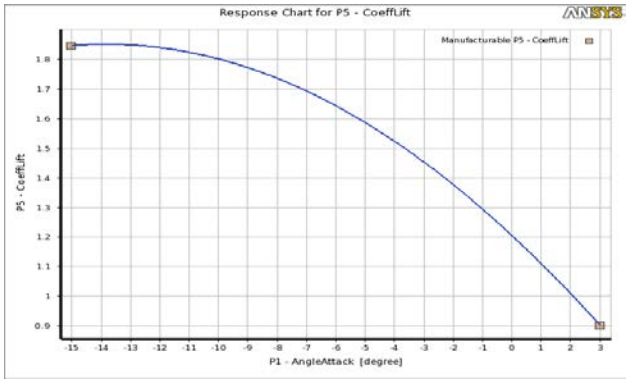

Figure 13: Polar graph: Cl vs α according to response surface. Stall angle at 13°. $C_{l_{max}} = 1.85$.

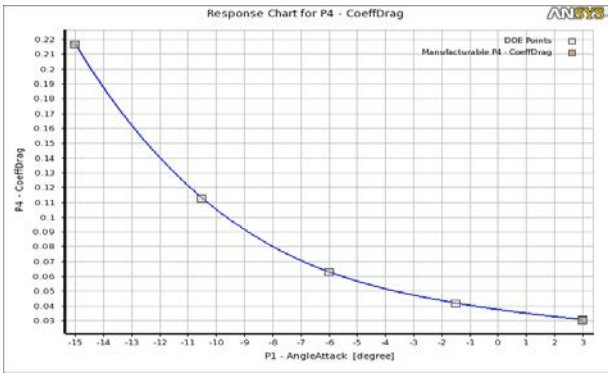

Figure 14: Polar graph: Cd vs α according to response surface.

Table 3 contains the critical angle and coefficients according to XFLR5, Fluent and the statistical analysis of response surface. It was defined that range between 12° and 14° is the critical position for the airfoil. There was a big difference in the value of the drag coefficient obtained by XFLR5, Fluent and response surface; while the lift coefficient presented similar values in CFD and the Response Surface, 1.9 and 1.85, respectively.

Table 3:Airfoil results from several simulations.

Case 1.	**XFLR5**	**Fluent**	**Surface Response**
α_{max}	14°	12°	13°
$C_{l_{max}}$	2.09	1.90	1.85
$C_{d_{max}}$	0,047	0,065	0.16

B. Case 2: Wing Geometry.

The second case involves the wing geometry of Cenzontle as an object of study. It is analyzed the behavior of the fluid in the wing geometry, the pressure distribution along the semi-wingspan of the wing and the variation of the aerodynamic coefficients in order to determine the load capacity of the wing

geometry. With the results of the CFD simulation it can be seen that the fluid presents a laminar behavior, orderly and without disturbances on the wing geometry except in the region near the wingtips as shown in Figure 15.

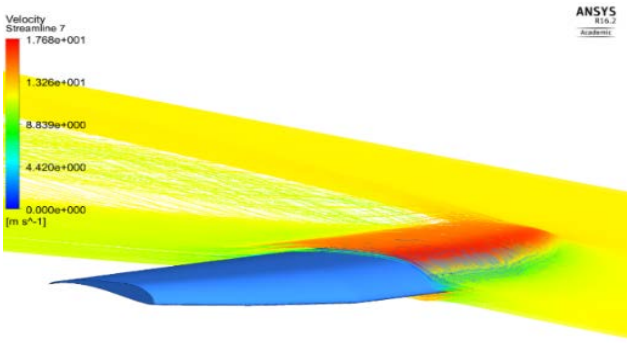

Figure 15: Streamlines of velocity 3D wing geometry.

Since it is a finite geometry, vortexes are generated at the tip of the wing due to the difference in speeds. These vortexes contribute to the increase of drag and decrease the lift of the wing. Because of this, it should be analyzed the possibility of deploying winglets to reduce the effects caused by the vortexes.

Figure 15° show the wing with 3° of incidence, where the air over the wing area reaches a maximum speed of 17.6 m/s, value that decreases with respect to the 19.4 m/s estimated for the airfoil analyzed in 2D. The contours of pressure seen in Figures 16 and 17 show the static pressure in the lower and upper surfaces of the aircraft respectively. The region of higher lift is located on the central section of the wing. The contours are clearly defined, however, in the wing tips, the contours begin to be limited due to the vortexes generated in that region. The distribution and pressure differentials are similar in the center section and the first trapezoidal area, while in the second change of geometry appears a distribution affected by the amount of fluid that moves from the lower surface toward the upper surface.

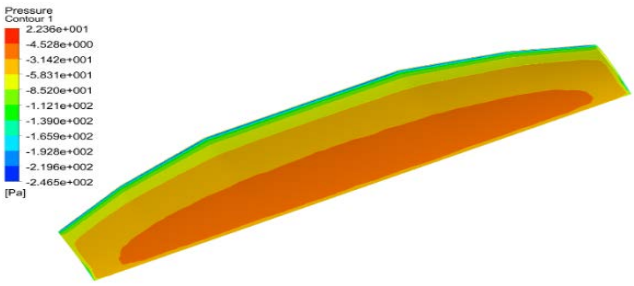

Figure 16: Contours of pressure in the lower surface.

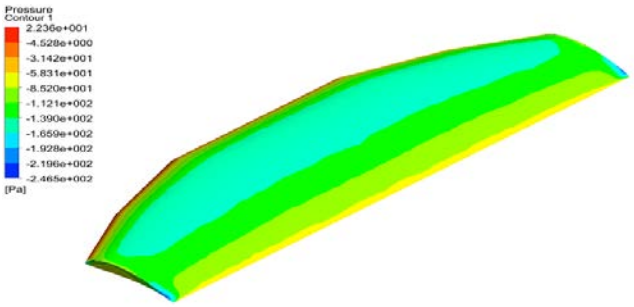

Figure 17: Upper surface contours of pressure.

Figure 18 shows a comparison of the pressure on both sides of the wing area along the semi-wingspan. The pressure values were estimated in three different positions: 25%, 30% and 35% of the chord of the airfoil. In all three positions the same pattern is observed, large differentials of pressures from the root to the half of the second change of geometry, with a gradual decrease in the last 0.15 m.

Of the three positions, C25% presents a lower pressure difference in the rectangular area of the wing, while the pressure values for C30% and C35% are nearby in practically all of the semi-wingspan. C30% was taken as reference for center of pressure, since it shows a better behavior in the tip of the wing than the other two graphed positions. The pressure on the upper surface keeps between -155 Pa and -160 Pa, in the first two sections, while in the last section it starts out with a value of -155 Pa, decreasing in the last 0.15 m of the wingspan until reaching the pressure of the lower surface. For its part, the pressure in the lower surface varies from -40 Pa in the root to the -50 Pa in the second change of geometry, showing a significant decrease in the last 0.1 m wingspan. The area that is affected by the fluid exchange represents about 15% of the wing area. The greater aspect to consider is the control of the ailerons, which are located in the wing tips and will see a 35% of its surface affected by this phenomenon.

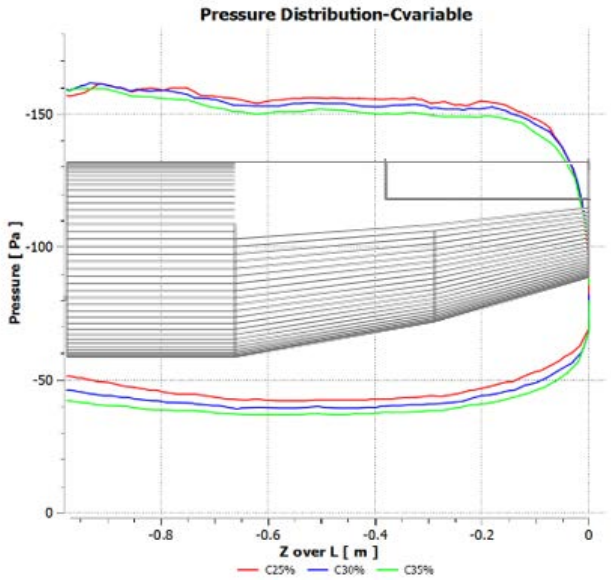

Figure 18: Comparison of pressure distribution at 25%, 30% and 35%.

To identify the behavior of the lift and drag coefficients of the wing in relation to the angle of incidence, a statistical model of response surface was used. The polar graph Cl vs and Cd vs are shown in Figures 19 and 20 respectively. An operating range of -13° to 3°, was delimited taking into account stall condition of the airfoil, since the rotation point of the wing is considered in the leading edge, negative values of in the charts represent a positive incidence of the wing.

The Cl reaches up to a maximum of 13° with a value of 1.78, while when =0° it is estimated a Cl of 0.85. The Cl_{max} is equivalent to a lifting force of 118 N at =13° as shown in Figure 21. The variation of the drag force is shown in Figure 22. The drag coefficient presents a Cdmax of 0.24 when =13° and 0.06 with 0°.

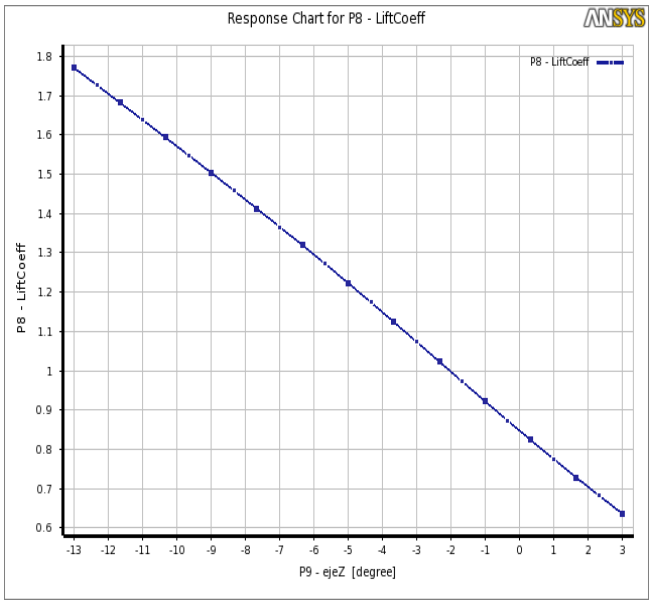

Figure 19: Cl vs .

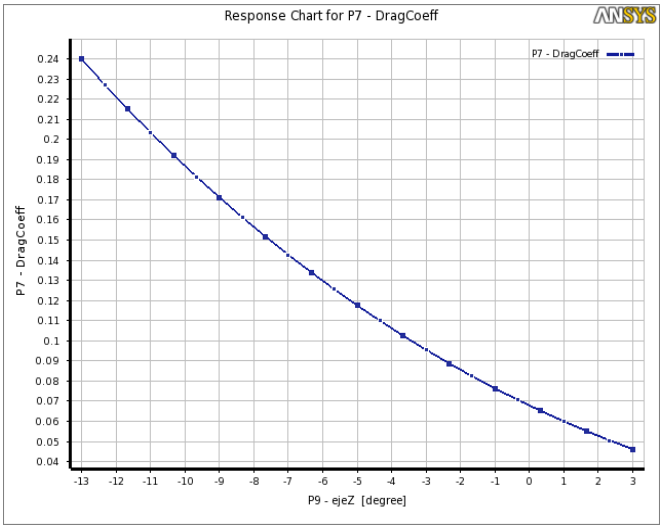

Figure 20: Cd vs .

The response surface model is used to determine the variation of both coefficients when rotating the wing respect to any of its axes. The behavior of the Cl is similar in different angles of attack as shown in Figures 23 and 24, which represent the Cl variation upon rotating the wing geometry at two specific angle of attack, 3° and 13° respectively. The Cl_{max} is reached while the wing stays in position of straight and leveled flight, without any rotation and reaches its minimum value when it is turned 30° on both axes. The Cl begins to decrease as it starts the roll or yaw movements, as for example, with an incidence of 13°, the Cl decreases to 1.57 if there is a rolling of 30°, while in a yaw movement with the same angle the Cl presents a value of 1.32.

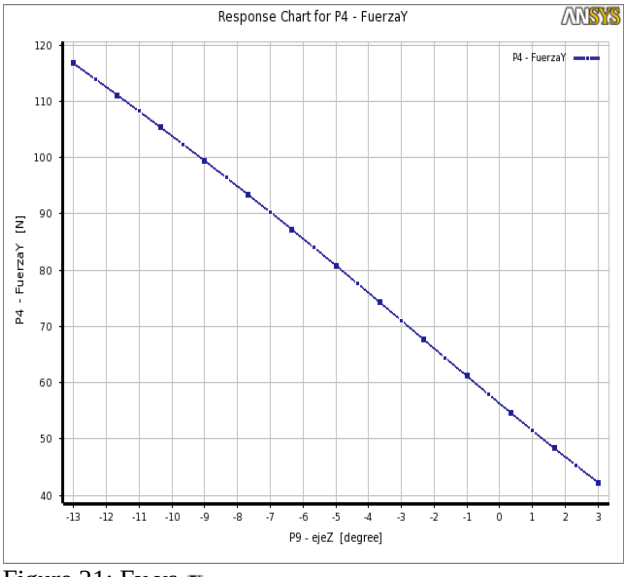

Figure 21: Fy vs .

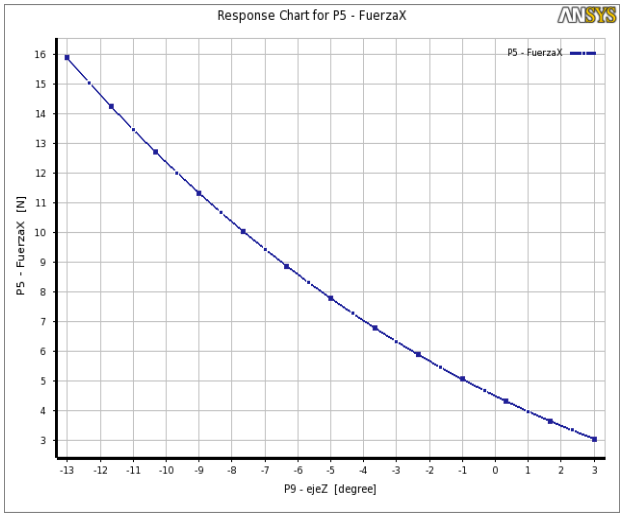

Figure 22: Fx vs α.

While it is true that the higher angle of attack reaches larger coefficients before the stall, it also presents more drastic changes at the time of rotating the wing geometry. When the wing has an incidence of 13° it presents a Cl of 1.75 which drops 0.2 on a 30° roll maneuver, while in a yaw, the Cl drops to 0.45 with the same rotation angle. On the other hand, with an incidence of 3°, the Cl_{max} is only 1.05, but it only presents a decrease of 0.13 and 0.28 for similar maneuvers. This means that it is necessary to increase the speed of the aircraft in order to keep a level flight in turns. Table 4 shows the required speeds for several positions according to rotation angles and wing incidence.

Considering an initial position (1) of the aircraft with an incidence of 3°, the wing generates a lift force of 117 N. So in order to keep the airframe at the same incidence in the final position (4), it is necessary to increase the speed around 4 m/s from position (1), until around 19.3 m/s. On the other hand, if the aircraft is flying at 13° of incidence, the required speed for the first position is 12.1 m/s, and just 14.8 m/s if there is a roll and yaw maneuver of 30° each (4).

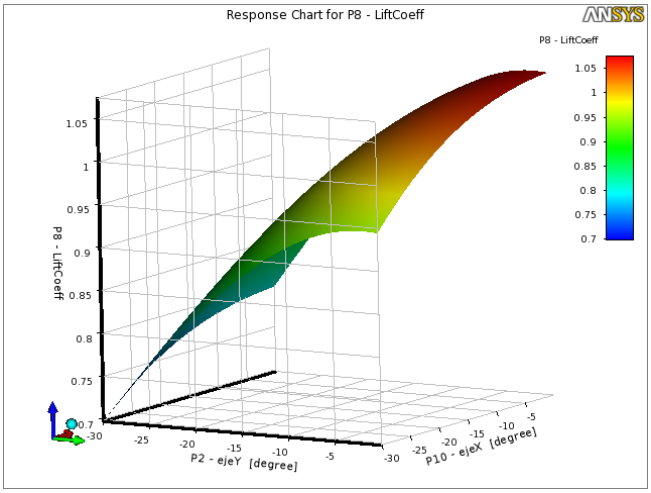

Figure 23: Lift coefficient (Cl) variation for roll and yaw maneuvers at α= 3°.

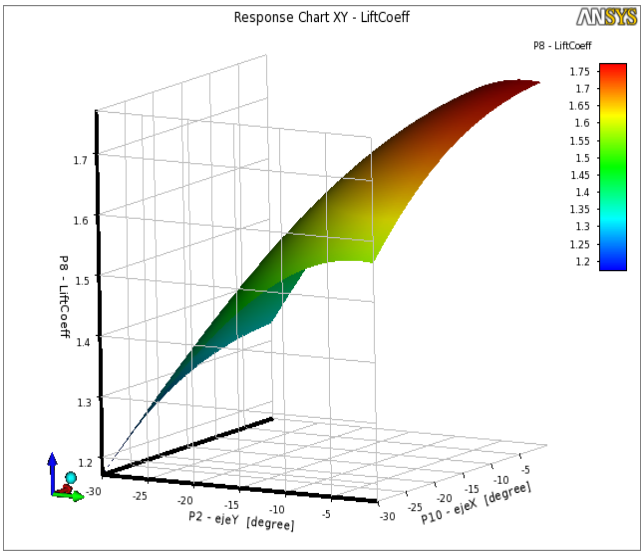

Figure 24: Lift coefficient (Cl) variation for rall and yaw maneuvers at α= 13°.

Maintaining a constant speed of 12 m/s the lift force of the aircraft decreases similarly as the Cl, as shown in Fig. 23 to Fig. 26 for 3° and 13° angle of attack. The greatest difference of lift force (Fy) is presented at a higher incidence, for example, when the aircraft have an incidence of 13°, the diminution of Fy is approximately 40 N from level flight (1) to position 4 (see Table 4 for positions reference), while when =3°, the Fy drop is only 25 N.

Table 5 shows the obtained coefficients according to each of the methodologies. The theoretical correction by Anderson estimated a greater Cl and therefore a higher load capacity. For its part, the CFD simulations and analysis of response surface showed similar values for both lift and drag. To validate the theoretical results and approximations, the Cenzontle aircraft was tested within SAE Aero Design Brazil 2016 (Figure 27). This model recorded a maximum payload of 9.75 kg, which was close to the results obtained by CFD and RS.

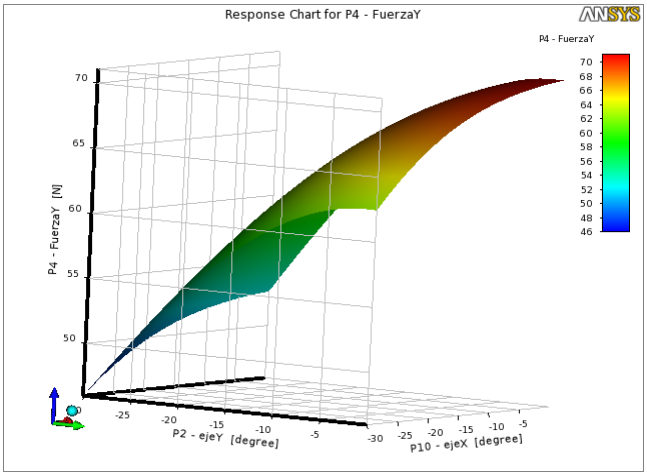

Figure 25: Lift force (LF) variation for roll and yaw maneuvers at α= 3°.

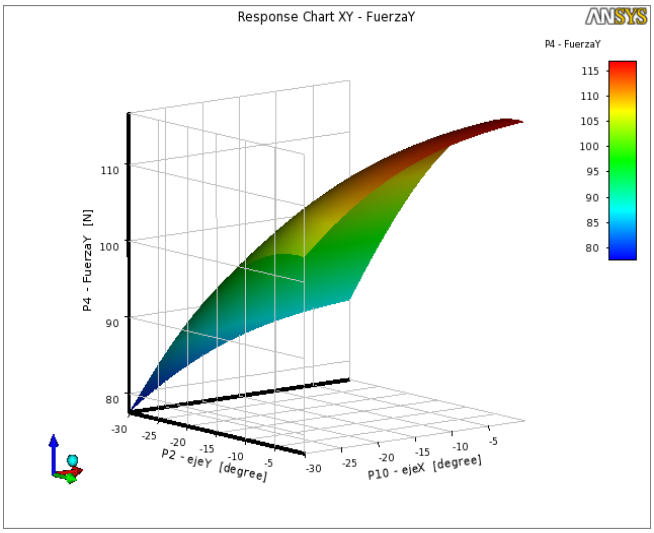

Figure 26: Lift force (LF) variation for roll and yaw maneuvers at α= 13°.

Table 4: Speed variation according to position.

P.	Rot. Angle		Cl		Speed (m/s)	
	X	Y	α=3°	α=13°	α=3°	α=13°
1	0	0	1.07	1.76	15.4	12.1
2	30	0	0.94	1.56	16.5	12.8
3	0	30	0.79	1.32	17.9	13.9
4	30	30	0.69	1.17	19.3	14.8

Table 5: Results comparative for 3D wing geometry.

Case 2.	Anderson	Fluent	Surface Response
$C_{L_{Max}}$	1.96	1.78	1.75
$C_{D_{Max}}$	0.27	0.24	0.23
F_{Lift}	120.8 N	118 N	117 N
Payload	10.1 kg	9.8 kg	9.7 kg

Figure 27: Aircraft Cenzontle during take-off.

IV. Conclusions.

The numerical values of Cl and Cd for the airfoil Pinefoil presented better results at 16 m/s than at 12 m/s, given that the Cl increases slightly while the Cd decreases in virtually all positions. Based on this, it is likely that the airfoil possibly presents a better performance at higher speeds and higher Reynolds numbers, however, its performance under the current operating conditions are satisfactory since the aerodynamic coefficients are similar to airfoils designed to operate under similar parameters.

Implementation of CFD tools and response surfaces (RS) allow predicting the dynamic-fluid behavior of the airfoil at specific flight conditions, as well as some of its main features, such as the stall angle, Cl_{max} and Cd. In addition, it is possible to estimate the payload capacity of the wing geometry and perform the relevant comparative between theoretical corrections of Cl and Cd and results obtained through simulations. The 3D simulations show that there is turbulence in the wingtips generated by the pressure differential, which could be reduced by adding winglets.

The use of response surfaces models (RS) and statistical approximations facilitates the analysis of the airfoil and wing geometry at several positions. Even though it is necessary to create enough design points in the critical positions in order to get a proper behavior of the variables under study. The CFD tools represent an option to estimate with good accuracy the payload capacity of an aircraft. However, it is necessary to analize all components of the aircraft, since each of them contributes in the total lift and drag of the model.

To increase the load capacity of the aircraft it is recommended the implementation of high lift devices, such as flaps and slats. For this specific case, the use of leading edge slats will help to reduce the pressure generated in the leading edge, which will reduce the generated drag.

Acknowledgment

To all Ufly team members from Universidad Aeronautica en Queretaro and staff members from Centro de Investigacion en Materiales Avanzados (CIMAV), especially to Rodrigo Dominguez due his support and availability of computer cluster cerberus.cimav.edu.mx.

REFERENCES

[1] Raymer, D. P. (1999). Aircraft design: a conceptual approach, American Institute of Aeronautics and Astronautics Vol. 21.

[2] Hiremath, S., and Malipatil, A. S. (2014). CFD Simulation of Aircraft Body with Different Angle of Attack and Velocity. International Journal of Innovative Research in Science, Engineering and Technology 3, 10. ISSN 2319-8753

[3] Triet, N. M., Viet, N. N., and Thang, P. M. (2015). Aerodynamic analysis of aircraft wing. VNU Journal of Science: Mathematics-Physics 31(2). https://js.vnu.edu.vn/MaP/article/view/111

[4] Ma, R., and Liu, P. (2009, July). Numerical simulation of low Reynolds number and high-lift airfoil S1223. In Proceedings of the World Congress on Engineering Vol. 2, pp. 1-3. https://pdfs.semanticscholar.org/2fe1/2d99a67df73fad013ae99741fbdbc4f07898.pdf

[5] Sethunathan, P. (2014). Computational Investigation of Inviscid Flow over a Wing With Multiple Winglets. International Journal of Engineering and Research Vol 3. ISSN 2278-0181

[6] Singh, J., Singh, D. J., Singh, A., Rana, A., and Dahiya, A. (2015). Study of NACA 4412 and Selig 12223 airfoils through computational fluid dynamics. SSRG International Journal of Mechanical Engineering (SSRG-IJME) vol 2. ISSN: 2348 – 8360 http://www.internationaljournalssrg.org/IJME/2015/Volume2-Issue6/IJME-V2I6P104.pdf

[7] Drela, M. (1989). XFOIL: An analysis and design system for low Reynolds number airfoils. In Low Reynolds number aerodynamics (pp. 1-12). Springer, Berlin, Heidelberg. http://web.mit.edu/drela/Public/papers/xfoil_sv.pdf

[8] Kontogiannis, S. G., Mazarakos, D. E., and Kostopoulos, V. (2016). Atlas IV wing aerodynamic design: From conceptual approach to detailed optimization. Aerospace Science and Technology 56, 135-147. DOI 10.1007/s10846-015-0325-9

[9] Yuksek, B., Vuruskan, A., Ozdemir, U., Yukselen, M. A., and Inalhan, G. (2016). Transition flight modeling of a fixed-wing VTOL UAV. Journal of Intelligent & Robotic Systems 84(1-4), 83-105.

[10] Anderson, J. D. (1999). Aircraft performance and design. McGraw-Hill Science/Engineering/Math.

[11] Miranda, L. (2011). Fundamentos da engenharia aeronáutica: Aplicações ao Projeto SAE-Aerodesign. Sao Paulo: Instituto Federal de Educacion.

[12] Sadraey, M. H. (2012). Aircraft design: A systems engineering approach. John Wiley & Sons.

[13] McClamroch, N. H. (2011). Steady aircraft flight and performance. Princeton University Press.

[14] Phillips, W. F. (2004). Mechanics of flight. John Wiley & Sons.

[15] Yechout, T. R. (2003). Introduction to aircraft flight mechanics. Aiaa.

[16] SAE Brasil, 18va Competicao SAE BRASIL AeroDesign 2016, SAE Brasil, 2016.

[17] Chen, J., Wang, Z., Zhang, J., Zhang, L., and Wu, G. (2015). Numerical Simulation for Changes in Aerodynamic Characteristics Along the Spanwise of “Diamond Back” Wing. Procedia Engineering, 99, 566-574. https://doi.org/10.1016/j.proeng.2014.12.572

[18] Font Prats, P. (2013). Aerodynamic analysis of the lift reducer device by flow transfer. Bachelor's thesis, Universitat Politècnica de Catalunya. https://upcommons.upc.edu/handle/2099.1/22246

[19] Crivellini, A., and D’Alessandro, V. (2014). Spalart–Allmaras model apparent transition and RANS simulations of laminar separation bubbles on airfoils. International Journal of Heat and Fluid Flow, 47, 70-83. https://doi.org/10.1016/j.ijheatfluidflow.2014.03.002

[20] Ansys. (2013). Design Exploration User’s Guide, Ansys Inc. USA.

G. Salazar Jimenez. Born in Tehuacan, Puebla, Mexico on June 27th 1994. Professional education: Eng. Aeronautical Engineering 2017, Universidad Aeronautica en Queretaro, Mexico. Currently is enrolled in MSc. Aerospace Vehicle Design in Cranfield University, United Kingdom cohort 2017-2018.
He is interested in conceptual design for unmanned vehicles, through his bachelor degree, he participated in SAE Aerodesign Mexico 2014-2016 and USA 2015 & 2016. Besides, he is interested in new technologies for commercial aircraft, especially in drag reduction technologies.

Héctor Alfredo López-Aguilar born January 24th 1980 in Uruapan Michoacán, México.
Professional education: PhD in Environmental Science and Technology, Advanced Materials Research Center Chihuahua (CIMAV). Actually, his research activities are focused in CFD and combustion simulation, Mass Transport Phenomena and Energy, renewable energies, biomass and Life Cycle Assessment methodology.

Jorge Alberto Gómez, PhD in materials science. Born in Chihuahua, Chihuahua Mexico on July 3th 1974. Professional education: Industrial Engineer 2000, Technological Institute of Chihuahua. Master's and doctorate degree in materials science 2001 and 2008 respectively, CIMAV- Chihuahua. The relevant contributions in this subject is with the first paper "A Method to Evaluate the Tensile Strength and Stress–Strain Relationship of Carbon Nanofibers, Carbon Nanotubes, and C-chains" published in 2005 on SMALL, as several patents of nanomaterials devices. Actually, the research activities are focused in the lithography construction of the device, test "in situ" of carbon nanotubes employing the new device and study the mechanical properties of different types of carbons nanotubes as a different metallic catalyst on them.

Adriana Chazaro Zaharias, MSc. Born in Cordoba, Veracruz, Mexico on June 16th, 1970. Professional education: B. Eng. Computational Science 1992, ITESM Campus Queretaro, Queretaro, Mexico. M Sc. Electronic Engineering 1999, Purdue University, Indiana, USA.
She is with the Postgraduate Department in the Universidad Aeronautica en Queretaro teaching in Graduate courses since 2010. She has been developing projects for UNAQ in conjunction with Mexican Space Agency and CONACYT. Currently working in conceptual design for microgravity vehicles.
Mrs. Chazaro is member of Society of Automotive Engineers since 2014, has been participating as faculty advisor of UNAQ representative team in SAE Collegiate Design Series in Mexico, USA and Brazil.

Jose Alberto Duarte Moller, Ph. D. Born in Guaymas Sonora, Mexico on March the 27th, 1967. Professional education: B. Sc. Physics 1990, Physics Department, University of Sonora, Hermosillo Sonora, México,. M Sci. Physics of Materials 1993. Applied Physics Department, CICESE, Ensenada BC. Mexico, Ph D. Physics of Materials 1996. Applied Physics Department, CICESE, Ensenada BC. Mexico. Posdoctorate on Nanotechnology 2002, Chemistry Department University of Texas at El Paso, El Paso TX, USA

Antonino Pérez Hernández, PhD. Born in Gutierrez Zamora Veracruz, Mexico on January the 9th, 1963. Professional education: B. Sc. Physics 1987, Faculty of Physical and Mathematical Sciences, Autonomous University of Nuevo León, San Nicolás de los Garza Nuevo León, México. M Sci. in Mechanical Engineering with Specialization in Materials 1992, FIME-UANL, Ph Materials Engineering 1994, FIME-UANL
Actually, the research activities: Applied Mathematics: Models of Physical Phenomena, Chemicals and Transfer. Process Simulation: Combustion, Filtration. Mass Transport Phenomena and Energy. Alternative Energy: Biomass, Bioelectricity, Hazardous Waste. Life Cycle Assessment (LCA). Human Resources Training.